AlScN/n-GaN Ferroelectric Memristors With Controllable On/Off Ratios and Reversible Bipolar Resistive Switching Characteristics

Mingrui Liu, Shunpeng Lu, Yuping Jia, Hang Zang, Ke Jiang, Xiaojuan Sun, and Dabing Li

***Abstract*— AlScN-based memristors show high potential of non-volatile storage and neuromorphic computing. Here, we report an AlScN/n-GaN heterostructure memristor with a large ON/OFF ratio over 10^5 attributed to the coexistence of heterointerface energy band modulation and trap-assisted conduction mechanisms. Unlike typical ferroelectric memristors, the device presents obvious reproducible bipolar resistive switching characteristics without polarization flipping due to the extra trap-assisted conductive path, which effectively reduces energy consumption. Remarkably, multi-level ON/OFF ratios and reversible bipolar resistive switching characteristics can be achieved by regulating the magnitude and direction of ferroelectric polarization, indicating that different operating modes can be achieved on a single device, which shows promise for improving device integration density and information security. These findings help elucidate the resistive switching mechanism and the effect of ferroelectric polarization on device properties, which pave the way for applications of power-efficient CMOS-compatible nitride memristors.**

***Index Terms*— AlScN/n-GaN, ferroelectric controllable, memristors.**

I. Introduction

FERROELECTRIC memristors are one of the most promising candidates for neuromorphic computing, which can potentially overcome the speed and power consumption bottlenecks imposed by conventional von Neumann systems [1], [2]. Recently, wurtzite-structured AlScN has attracted wide attention due to its combination of the excellent ferroelectric properties and advantages of wide-bandgap nitride materials. AlScN bears high remnant polarizations (P_r, of 80-150 μC/cm), a low synthesizing temperature (< 400 °C), and a high Curie temperature (T_c, up to 1100 °C) [3], [4], [5], [6]. The P_r is more than 2–6 times that of HfO_2 or perovskite ferroelectrics [7], which results in a stronger barrier regulation ability and a larger ON/OFF ratio than other ferroelectric memristors [8], [9], [10], [11]. The low synthesizing temperature and high T_c make AlScN attractive for applications in back-end-of-line CMOS-compatible memristors and ensure its stability in extreme environments. Furthermore, the integration process of AlScN memristors onto well-established nitride optoelectronic and microelectronic devices [12], [13], [14] is straightforward, which is essential to realize the integration of multifunctional nitride devices.

However, AlScN-based memristors are still in their infancy. The resistive switching is mainly attributed to the strong barrier modulation caused by polarization flipping [15], [16], [17], which is not power-efficient due to its large coercive fields (E_c, of 2-8 MV/cm) [6]. In addition, the tunable ferroelectric depolarization field (E_{DP}) can efficiently modulate the transport of electron and nitrogen vacancies [18], [19], [20], [21], which may affect memristor properties and should be further explored.

In this letter, we introduced a suitable defect density in AlScN by controlling the sputtering temperature and fabricated an AlScN/n-GaN heterostructure memristor. Interestingly, the device exhibits reproducible bipolar resistive switching characteristics without polarization flipping. The resistive switching mechanism and the effect of ferroelectric polarization on memristor properties were systematically studied both experimentally and theoretically.

II. Experimental Section

$Al_{0.75}Sc_{0.25}N$ films were prepared on n-GaN/sapphire templates by RF-reactive magnetron sputtering from a metal alloy target in pure N_2 with a chamber pressure of 0.7 Pa. The defect density can be controlled by the deposition temperature, and the samples grown at 400°C have a suitable defect density and good repeatability. The thickness of the AlScN film was 170 nm, and the bottom Si-doped n-GaN contact layer was 2 μm with a carrier density higher than 10^{19} cm^{-3}, which can be used as the bottom electrode (BE). Au/Ti (30/70 nm) top electrodes (TE) with diameters of 100 μm were deposited

Manuscript received 16 November 2023; revised 8 December 2023 and 19 December 2023; accepted 21 December 2023. Date of publication 25 December 2023; date of current version 27 February 2024. This work was supported in part by the National Key Research and Development Program of China under Grant 2022YFB3605600, in part by the National Natural Science Foundation of China under Grant 62121005 and Grant 12204475, and in part by the Youth Growth Science and Technology Program of Jilin Province under Grant 20220508018RC. The review of this letter was arranged by Editor G. H. Jessen. *(Corresponding author: Dabing Li.)*

Mingrui Liu, Shunpeng Lu, Yuping Jia, Hang Zang, Ke Jiang, and Xiaojuan Sun are with the State Key Laboratory of Luminescence and Applications, Changchun Institute of Optics, Fine Mechanics and Physics, Chinese Academy of Sciences, Changchun 130033, China.

Dabing Li is with the State Key Laboratory of Luminescence and Applications, Changchun Institute of Optics, Fine Mechanics and Physics, Chinese Academy of Sciences, Changchun 130033, China, and also with the Center of Materials Science and Optoelectronics Engineering, University of Chinese Academy of Sciences, Beijing 100049, China (e-mail: lidb@ciomp.ac.cn).

Color versions of one or more figures in this letter are available at https://doi.org/10.1109/LED.2023.3347233.

Digital Object Identifier 10.1109/LED.2023.3347233

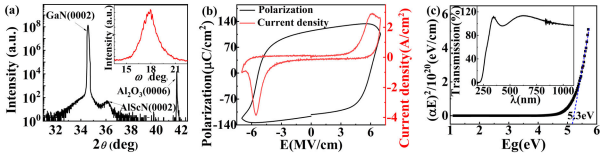

Fig. 1. (a) XRD patterns and (0002) rocking curves for the AlScN film. (b) Polarization/displacement current density variations with electric fields were collected by Radiant Precision Premier II ferroelectric tester at 1 kHz. (c) Optical transmission spectra and dependence of $(\alpha E)^2$ on Eg of the AlScN film.

by electron beam evaporation. Inset Fig. 2(a) is the schematic diagram of the device.

III. Results and Discussions

Fig. 1(a) shows the X-ray diffraction (XRD) data of a wurtzite-structure AlScN film. Inset is the rocking curve of the (0002) peak with a 1.73°full width at half maximum (FWHM), and the defect density was calculated as 8.4×10^{10} cm^{-2}. The ferroelectricity of the AlScN film is confirmed in Fig. 1(b), the E_c is 5.8 MV/cm, and the P_r is 110 μC/cm^2. The bandgap (Eg) of the AlScN film is 5.3 eV, as shown in Fig. 1(c).

First, we applied a positive write voltage (100 V, 10 ms) which is higher than the coercive voltage (V_c) to the TE to make the ferroelectric polarization of AlScN downward towards n-GaN (P_{down}). In Fig. 2(a), the Au/Ti/AlScN/n-GaN device shows counterclockwise bipolar resistance switching behaviour. As the voltage increases from 0 V to "+V", the programming current increases gradually and switches from a high-resistance state (HRS, or OFF state) to a low-resistance state (LRS, or ON state), then switches back to HRS when applying a "-V". Furthermore, multi-level programming currents emerge with an increasing voltage range from 10 to 40 V, which is essential for high-density data storage and neuromorphic computing [22]. Note that the applied voltage is more than 65% [the "write" voltage is 20 V, and the V_c measured by the quasi-DC sweep is 58 V (not shown)] lower than the V_c, indicating the device exhibits bipolar resistive switching characteristics without polarization flipping, which is essential to reduce energy consumption. Fig. 2(b) shows the programming current of HRS and LRS at 5 V extracted from Fig. 2(a). The programming current increases with the applied voltage increase, especially for LRS, which results in an order of magnitude increase in the ON/OFF ratio and reaches 5.3×10^3 at 40 V. Inset Fig. 2(c) shows the current-voltage (I-V) curves from 10 manually performed 40 V DC cycles, which indicate that the device is stable and repeatable. As shown in Fig. 2(c), the retention properties were 10^3 s measured at a read voltage of 5 V after a write voltage of 40 V.

Furthermore, the large Eg and suitable permittivity of the AlScN film lead to better insulation properties [23], hence, the device exhibits a satisfactorily low programming current of less than 2×10^{-7} A (the current flow through the device during "set" operation [21]) without additional access transistors or selectors, which will help suppress the sneak current in the crossbar array, simplify the integration steps, and reduce device power consumption [21], [22], [23], [24], [25]. A comparison of the AlScN/n-GaN memristor with others is shown in Fig. 2(d) , [11], [15], [17], [25], [26], [27], [28], [29], [30], we used the programming current times thickness divided by area and converted it to resistivity in order to eliminate the effects of device thickness and area. The difference in

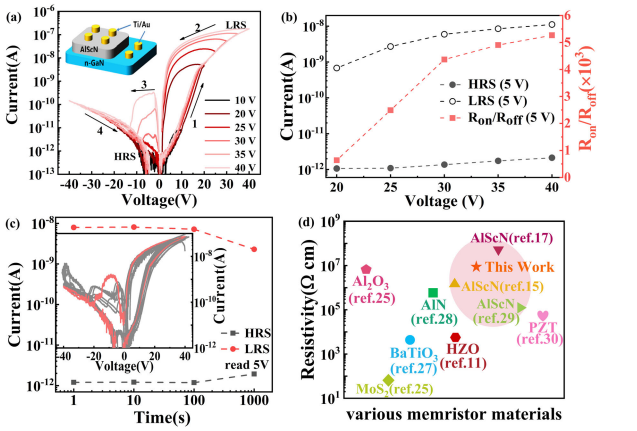

Fig. 2. (a) Bipolar resistive switching characteristics under a DC voltage sweep on the device; inset is the schematic of the device structure. (b) The programming currents of HRS and LRS and ON/OFF ratio versus the applied voltages. (c) Retention properties of the low and high current for 10^3 s, by the readout at 5 V, Inset: 10 cycles of I-V curves performed at 40 V. (d) The comparison for programming resistivity.

resistivities among other AlScN memristors is caused by the different composition of Sc, which leads to a different Eg [23].

To study why the resistance can be switched without polarization flipping, we analyzed the I−V curve according to transport mechanisms. In Fig. 3(a), when the applied voltage increases from 0 to 5 V, the current density (J_F) can be fitted by the thermionic emission mechanism (Equation 1), which means that Schottky barriers dominate the transport [27], [31]:

$$J_F = A^* T^2 \exp\left[\frac{-q(\phi_B - \sqrt{qE/4\pi\varepsilon})}{K_B T}\right] \quad (1)$$

where A^* is the effective Richardson constant, T is the absolute temperature (300 K), K_B is the Boltzmann constant, ϕ_B is the Schottky barrier height, ε is the permittivity, and q is the electron charge. When the applied voltage is further increased until the device reaches a LRS, the I−V curve can be well-fitted by the Trap-assisted tunneling (TAT) model (Equation 2) [31]:

$$J_F = A \exp\left(\frac{-8\pi\sqrt{2qm^*}}{3hE}\phi_T^{3/2}\right) \quad (2)$$

where A is a constant and ϕ_T is the energy of the electron traps with respect to the conduction band edge. These results indicate that more than one mechanism leads to the resistance switching. Note that the defects densities of the sputter deposited AlScN film are two orders of magnitude higher than those grown by MBE [32], [33], [34], [35], these defects cause trap states in the bandgap, as shown in Fig. 3(b). Hence, in addition to the barrier modulation by ferroelectric polarization, the effect of the E_{DP} on electron hopping among traps should also be considered.

Fig. 3(c) shows the band offset diagram of the device. As illustrated in Fig. 3(d), in the case of P_{down}, the band of AlScN is tilted towards the BE. The positive polarization charges at the AlScN/n-GaN interface result in a downward bending of the n-GaN band profile and form an electron accumulation region. When "-V" ($< V_c$) is applied to the TE, the external electric field (E_{appl}) is in the same direction as the E_{DP} of AlScN, the positively charged nitrogen-vacancy (V_N^+) traps [18] tend to distribute near the TE, and the trap assisted conduction path is ruptured. Electron transport can only overcome the high barrier ϕ_1, showing a HRS. In Fig. 3(e), when

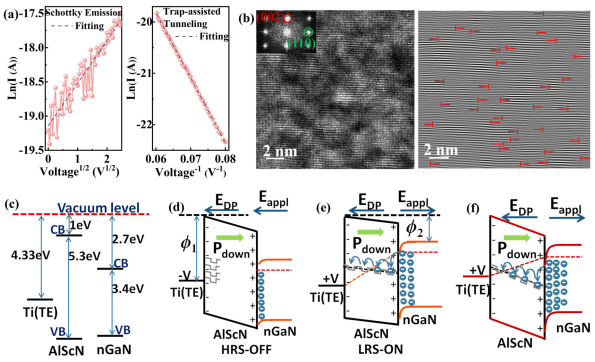

Fig. 3. (a) Fitting of experimental I-V data to the thermionic emission mechanism (left) and TAT model (right). (b) Left: High-resolution transmission electron microscope images for the AlScN film, inset is the fast Fourier transform (FFT); Right: Inverse FFT and the dislocations are marked. (c) The band offset diagram of the device. Schematic band structures of the HRS (d) and LRS (e) in the case of P_{down}. (f) Schematic band structures modulated by the magnitude of ferroelectric polarization in AlScN at LRS. It is assumed that the trap levels are at mid-gap.

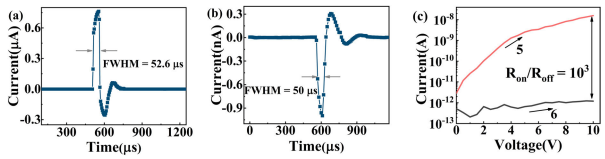

Fig. 4. ON (a) and OFF (b) switching using a 50 μs voltage pulse. (c)I-V curves after a short write pulse.

applying a "+V" on the TE, the direction of the E_{appl} is opposite to the E_{DP}, which is beneficial for the V_N^+ traps to move towards the BE and form the conductive path. On the one hand, electrons hop from highly occupied traps to empty traps, which obey TAT [31]. On the other hand, the electron barrier $\phi_2$is much lower than the barrier ϕ_1. Therefore, the device switches from HRS to LRS and exhibits rectification characteristics where the current at "+V" is greater than that at "-V". Furthermore, comparing Fig. 3(f) with (e), the magnitude of ferroelectric polarization in AlScN increases with the increase of the "+V", the downward bending degree of the n-GaN band profile becomes more prominent, and more electrons are attracted to the AlScN/n-GaN interface. Correspondingly, the Fermi level gradually moves upward [red dotted lines in Fig. 3(f)], and electrons are more likely to fill the defect traps, which benefits for the formation of conductive paths and electrons hopping. Therefore, multi-level programming current can be established by gradually increasing the magnitude of ferroelectric polarization and resulting in a tunable ON/OFF ratio.

Fig. 4 (a) and (b) shows the ON/OFF switching times under a short write pulse. The device was set to a HRS after the voltage sweeping in the Fig. 2(a) (process 1 to 4). Then, a "+40 V" pulse with a width of 50 μs was applied to the TE. The large current change from 10^{-12} A to 7.6×10^{-7} A with a FWHM of 52.6 μs can be observed in Fig. 4 (a). Later, when we performed the 0→"+ 10 V" sweeping voltage again, the current remained in a LRS [Fig. 4(c) process 5], which suggested that the 50 μs positive write voltage was sufficient to turn on the device. Correspondingly, the current could be successfully set to HRS with a switching time of 50 μs by applying a "−40 V" pulse, as shown in Fig. 4 (b) and process 6 in Fig. 4 (c). In fact, according to the previous report, the movement of nitrogen vacancy has ultra-fast speed and achieved a switching time of 85 ps in the AlN memristor [18], meaning that the device in this work may have the potential to achieve a shorter switching time. Unfortunately, we could not measure a pulse width of less than 50 μs due to the resolution limits of the PDA FS380 Pro semiconductor analyzer. But we believe that the AlScN/nGaN memristors will have higher speed and lower energy if we further optimize the device structure, such by reducing the thickness and device area.

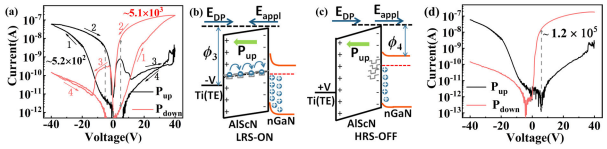

Fig. 5. (a) Bipolar resistive switching characteristics for P_{up} (black) and P_{down} (red). Schematic band structures of the LRS (b) and HRS (c) in the case of P_{up}. (d) Typical I-V characteristics for P_{up} and P_{down}.

Furthermore, the effect of ferroelectric polarization direction on resistance switching is also investigated. We applied a negative voltage (−100 V, 10 ms) to the TE to make the ferroelectric polarization of AlScN upward towards TE (P_{up}). Interestingly, the bipolar resistive switching characteristics were reversed as shown in Fig. 5 (a). In the case of P_{up}, the band of AlScN is tilted towards the TE, the negative polarization charges at the AlScN/n-GaN interface will repel electrons, leading to an upward bending of the n-GaN band profile as well as a depletion region, as shown in Fig. 5(b) and (c). When applying a "-V" ($< V_c$) on the TE, the E_{DP} of AlScN is weakened by the E_{appl}, and V_N^+ traps gradually move towards the BE to form the conductive path, showing an LRS. On the contrary, applying a "+V" leads to a rupture of the conduction path, the device switches from the LRS to HRS and exhibits rectification characteristics where the current at "+V" is lower than that at "−V", as shown by the black date line in Fig. 5(a). However, compared to Figs. 3(d) and (e), the ON/OFF ratio for P_{down} is one order of magnitude larger than that of P_{up} due to the different barrier heights ($\phi_3 > \phi_2$, $\phi_4 < \phi_1$). To further compare the ON/OFF ratio caused by the polarization flipping [15], we extracted the I-V curves of P_{up} and P_{down} from Fig. 5(a). In Fig. 5(d), the ON/OFF ratio read at 5.7 V is more than 10^5, which is three orders of magnitude larger than that reported by Ding Wang et al. [15]. Such a large ON/OFF ratio is the result of the coexistence of semiconductor-ferroelectric heterointerface energy band modulation and TAT mechanisms.

IV. Conclusion

In summary, we fabricated an Au/Ti/AlScN/n-GaN heterostructure memristor with a large ON/OFF ratio over 10^5, due to the coexistence of TAT and semiconductor-ferroelectric heterointerface energy band modulation machinisms. Without polarization flipping, the device presents bipolar resistive switching characteristics with the applied voltage being more than 65% lower than the V_c. Furthermore, the controllable ON/OFF ratio and reversible bipolar resistive switching characteristics indicate that resistance switching can be regulated by both the magnitude and direction of ferroelectric polarization. These results facilitate a deeper understanding of the resistive switching mechanism and the role of ferroelectric polarization in AlScN memristors. However, it has to be admitted that the V_N^+defects sacrifice the retention characteristic to a certain degree, which suggests that the performance of the device has further room for improvement.

REFERENCES

[1] M. Tarkov, F. Tikhonenko, V. Popov, V. Antonov, A. Miakonkikh, and K. Rudenko, "Ferroelectric devices for content-addressable memory," *Nanomaterials*, vol. 12, no. 24, p. 4488, Dec. 2022, doi: 10.3390/nano12244488.

[2] C. Wang, A. Agrawal, E. Yu, and K. Roy, "Multi-level neuromorphic devices built on emerging ferroic materials: A review," *Frontiers Neurosci.*, vol. 15, Apr. 2021, Art. no. 661667, doi: 10.3389/fnins.2021.661667.

[3] S. Yasuoka, T. Shimizu, A. Tateyama, M. Uehara, H. Yamada, M. Akiyama, Y. Hiranaga, Y. Cho, and H. Funakubo, "Effects of deposition conditions on the ferroelectric properties of $(Al_{1-x}Sc_x)N$ thin films," *J. Appl. Phys.*, vol. 128, no. 11, Sep. 2020, Art. no. 114103, doi: 10.1063/5.0015281.

[4] M. R. Islam, N. Wolff, M. Yassine, G. Schönweger, B. Christian, H. Kohlstedt, O. Ambacher, F. Lofink, L. Kienle, and S. Fichtner, "On the exceptional temperature stability of ferroelectric $Al_{1-x}Sc_xN$ thin films," *Appl. Phys. Lett.*, vol. 118, no. 23, Jun. 2021, Art. no. 232905, doi: 10.1063/5.0053649.

[5] P. Wang, D. Wang, N. M. Vu, T. Chiang, J. T. Heron, and Z. Mi, "Fully epitaxial ferroelectric ScAlN grown by molecular beam epitaxy," *Appl. Phys. Lett.*, vol. 118, no. 22, May 2021, Art. no. 223504, doi: 10.1063/5.0054539.

[6] S. K. Ryoo, K. D. Kim, H. W. Park, Y. B. Lee, S. H. Lee, I. S. Lee, S. Byun, D. Shim, J. H. Lee, H. Kim, Y. H. Jang, M. H. Park, and C. S. Hwang, "Investigation of optimum deposition conditions of radio frequency reactive magnetron sputtering of $Al_{0.7}Sc_{0.3}N$ film with thickness down to 20 nm," *Adv. Electron. Mater.*, vol. 8, no. 11, Nov. 2022, Art. no. 2200726, doi: 10.1002/aelm.202200726.

[7] T. Mikolajick, U. Schroeder, and S. Slesazeck, "The past, the present, and the future of ferroelectric memories," *IEEE Trans. Electron Devices*, vol. 67, no. 4, pp. 1434–1443, Apr. 2020, doi: 10.1109/TED.2020.2976148.

[8] T. Choi, S. Lee, Y. J. Choi, V. Kiryukhin, and S.-W. Cheong, "Switchable ferroelectric diode and photovoltaic effect in $BiFeO_3$," *Science*, vol. 324, no. 5923, pp. 63–66, Apr. 2009, doi: 10.1126/science.1168636.

[9] P. Maksymovych, S. Jesse, P. Yu, R. Ramesh, A. P. Baddorf, and S. V. Kalinin, "Polarization control of electron tunneling into ferroelectric surfaces," *Science*, vol. 324, no. 5933, pp. 1421–1425, Jun. 2009, doi: 10.1126/science.1171200.

[10] R. Berdan, T. Marukame, K. Ota, M. Yamaguchi, M. Saitoh, S. Fujii, J. Deguchi, and Y. Nishi, "Low-power linear computation using nonlinear ferroelectric tunnel junction memristors," *Nature Electron.*, vol. 3, no. 5, pp. 259–266, May 2020, doi: 10.1038/s41928-020-0405-0.

[11] Q. Luo, Y. Cheng, J. Yang, R. Cao, H. Ma, Y. Yang, R. Huang, W. Wei, Y. Zheng, T. Gong, J. Yu, X. Xu, P. Yuan, X. Li, L. Tai, H. Yu, D. Shang, Q. Liu, B. Yu, Q. Ren, H. Lv, and M. Liu, "A highly CMOS compatible hafnia-based ferroelectric diode," *Nature Commun.*, vol. 11, no. 1, pp. 1391–1398, Mar. 2020, doi: 10.1038/s41467-020-15159-2.

[12] D. Li, K. Jiang, X. Sun, and C. Guo, "AlGaN photonics: Recent advances in materials and ultraviolet devices," *Adv. Opt. Photon.*, vol. 10, no. 1, pp. 43–110, Mar. 2018, doi: 10.1364/AOP.10.000043.

[13] M. Yang, M. Chong, D. Zhao, X. Wang, Y. Su, J. Sun, and X. Sun, "Back-illuminated $Al_xGa_{1-x}N$-based dual-band solar-blind ultraviolet photodetectors," *J. Semiconductors*, vol. 35, no. 6, Jun. 2014, Art. no. 064008, doi: 10.1088/1674-4926/35/6/064008.

[14] S. L. Selvaraj, A. Watanabe, A. Wakejima, and T. Egawa, "1.4-kV breakdown voltage for AlGaN/GaN high-electron-mobility transistors on silicon substrate," *IEEE Electron Device Lett.*, vol. 33, no. 10, pp. 1375–1377, Oct. 2012, doi: 10.1109/LED.2012.2207367.

[15] D. Wang, P. Wang, S. Mondal, S. Mohanty, T. Ma, E. Ahmadi, and Z. Mi, "An epitaxial ferroelectric ScAlN/GaN heterostructure memory," *Adv. Electron. Mater.*, vol. 8, no. 9, Sep. 2022, Art. no. 2200005, doi: 10.1002/aelm.202200005.

[16] D. Wang, P. Wang, S. Mondal, M. Hu, Y. Wu, T. Ma, and Z. Mi, "Ultrathin nitride ferroic memory with large ON/OFF ratios for analog in-memory computing," *Adv. Mater.*, vol. 35, no. 20, May 2023, Art. no. 202210628, doi: 10.1002/adma.202210628.

[17] P. Wang, D. Wang, S. Mondal, M. Hu, Y. Wu, T. Ma, and Z. Mi, "Ferroelectric nitride heterostructures on CMOS compatible molybdenum for synaptic memristors," *ACS Appl. Mater. Interfaces*, vol. 15, no. 14, pp. 18022–18031, Apr. 2023, doi: 10.1021/acsami.2c22798.

[18] B. J. Choi, A. C. Torrezan, J. P. Strachan, P. G. Kotula, A. J. Lohn, M. J. Marinella, Z. Li, R. S. Williams, and J. J. Yang, "High-speed and low-energy nitride memristors," *Adv. Funct. Mater.*, vol. 26, no. 29, pp. 5290–5296, Aug. 2016, doi: 10.1002/adfm.201600680.

[19] C. Chen, Y. C. Yang, F. Zeng, and F. Pan, "Bipolar resistive switching in Cu/AlN/Pt nonvolatile memory device," *Appl. Phys. Lett.*, vol. 97, no. 8, Aug. 2010, Art. no. 083502, doi: 10.1063/1.3483158.

[20] R. Prakash and D. Kaur, "Bipolar resistive switching behavior in Cu/AlN/Pt structure for ReRAM application," *Vacuum*, vol. 143, pp. 102–105, Sep. 2017, doi: 10.1016/j.vacuum.2017.05.041.

[21] X. Hou, R. Pan, Q. Yu, K. Zhang, G. Huang, Y. Mei, D. W. Zhang, and P. Zhou, "Tubular 3D resistive random access memory based on rolled-Up h-BN tube," *Small*, vol. 15, no. 5, Feb. 2019, Art. no. 180387, doi: 10.1002/smll.201803876.

[22] A. Chanthbouala, V. Garcia, R. O. Cherifi, K. Bouzehouane, S. Fusil, X. Moya, S. Xavier, H. Yamada, C. Deranlot, N. D. Mathur, M. Bibes, A. Barthélémy, and J. Grollier, "A ferroelectric memristor," *Nature Mater.*, vol. 11, no. 10, pp. 860–864, Oct. 2012, doi: 10.1038/NMAT3415.

[23] P. Wang, D. Wang, S. Mondal, M. Hu, J. Liu, and Z. Mi, "Dawn of nitride ferroelectric semiconductors: From materials to devices," *Semicond. Sci. Technol.*, vol. 38, no. 4, Apr. 2023, Art. no. 043002, doi: 10.1088/1361-6641/acb80e.

[24] X. Liu, J. Zheng, D. Wang, P. Musavigharavi, E. A. Stach, R. Olsson, and D. Jariwala, "Aluminum scandium nitride-based metal-ferroelectric-metal diode memory devices with high on/off ratios," *Appl. Phys. Lett.*, vol. 118, no. 20, May 2021, Art. no. 202901, doi: 10.1063/5.0051940.

[25] J. Zhou, F. Cai, Q. Wang, B. Chen, S. Gaba, and W. D. Lu, "Very low-programming-current RRAM with self-rectifying characteristics," *IEEE Electron Device Lett.*, vol. 37, no. 4, pp. 404–407, Apr. 2016, doi: 10.1109/LED.2016.2530942.

[26] R. Ge, X. Wu, M. Kim, J. Shi, S. Sonde, L. Tao, Y. Zhang, J. C. Lee, and D. Akinwande, "Atomristor: Nonvolatile resistance switching in atomic sheets of transition metal dichalcogenides," *Nano Lett.*, vol. 18, no. 1, pp. 434–441, Jan. 2018, doi: 10.1021/acs.nanolett.7b04342.

[27] Y. Yang, M. Wu, X. Li, H. Hu, Z. Jiang, Z. Li, X. Hao, C. Zheng, X. Lou, S. J. Pennycook, and Z. Wen, "The role of ferroelectric polarization in resistive memory properties of metal/insulator/semiconductor tunnel junctions: A comparative study," *ACS Appl. Mater. Interfaces*, vol. 12, no. 29, pp. 32935–32942, Jul. 2020, doi: 10.1021/acsami.0c08708.

[28] H.-D. Kim, H.-M. An, E. B. Lee, and T. G. Kim, "Stable bipolar resistive switching characteristics and resistive switching mechanisms observed in aluminum nitride-based ReRAM devices," *IEEE Trans. Electron Devices*, vol. 58, no. 10, pp. 3566–3573, Oct. 2011, doi: 10.1109/TED.2011.2162518.

[29] X. Liu, J. Ting, Y. He, M. M. A. Fiagbenu, J. Zheng, D. Wang, J. Frost, P. Musavigharavi, G. Esteves, K. Kisslinger, S. B. Anantharaman, E. A. Stach, R. H. Olsson, and D. Jariwala, "Reconfigurable compute-in-memory on field-programmable ferroelectric diodes," *Nano Lett.*, vol. 22, no. 18, pp. 7690–7698, Sep. 2022, doi: 10.1021/acs.nanolett.2c03169.

[30] L. Pintilie, V. Stancu, L. Trupina, and I. Pintilie, "Ferroelectric Schottky diode behavior from $aSrRuO_3$-$Pb(Zr_{0.2}Ti_{0.8})O_3$-tastructure," *Phys. Rev. B, Condens. Matter*, vol. 82, no. 8, Aug. 2010, Art. no. 085319, doi: 10.1103/PhysRevB.82.085319.

[31] E. Lim and R. Ismail, "Conduction mechanism of valence change resistive switching memory: A survey," *Electronics*, vol. 4, no. 3, pp. 586–613, Sep. 2015, doi: 10.3390/electronics4030586.

[32] D. Wang, P. Wang, S. Mondal, Y. Xiao, M. Hu, and Z. Mi, "Impact of dislocation density on the ferroelectric properties of ScAlN grown by molecular beam epitaxy," *Appl. Phys. Lett.*, vol. 121, no. 4, Jul. 2022, Art. no. 042108, doi: 10.1063/5.0099913.

[33] P. Wang, D. Wang, B. Wang, S. Mohanty, S. Diez, Y. Wu, Y. Sun, E. Ahmadi, and Z. Mi, "N-polar ScAlN and HEMTs grown by molecular beam epitaxy," *Appl. Phys. Lett.*, vol. 119, no. 8, Aug. 2021, Art. no. 082101, doi: 10.1063/5.0055851.

[34] P. Wang, D. A. Laleyan, A. Pandey, Y. Sun, and Z. Mi, "Molecular beam epitaxy and characterization of Wurtzite $Sc_xAl_{1-x}N$," *Appl. Phys. Lett.*, vol. 116, no. 15, Apr. 2020, Art. no. 151903, doi: 10.1063/5.0002445.

[35] P. Wang, D. Wang, Y. Bi, B. Wang, J. Schwartz, R. Hovden, and Z. Mi, "Quaternary alloy ScAlGaN: A promising strategy to improve the quality of ScAlN," *Appl. Phys. Lett.*, vol. 120, no. 1, Jan. 2022, Art. no. 012104, doi: 10.1063/5.0060608.